Acta Crystallographica Section D
Biological Crystallography
ISSN 1399-0047

Ligand-dependent active-site closure revealed in the crystal structure of *Mycobacterium tuberculosis* MenB complexed with product analogues

Haigang Song, Hoi Pang Sung, Yuk Sing Tse, Ming Jiang‡ and Zhihong Guo*

Department of Chemistry and State Key Laboratory of Molecular Neuroscience, The Hong Kong University of Science and Technology, Clear Water Bay, Kowloon, Hong Kong SAR, People's Republic of China

‡ Current address: State Key Laboratory of Microbial Metabolism, School of Life Sciences and Biotechnology, Shanghai Jiao Tong University, Shanghai 200240, People's Republic of China.

Correspondence e-mail: chguo@ust.hk

Received 14 June 2014
Accepted 27 August 2014

PDB references: MenB, complex with salicylyl-CoA, 4qii; complex with 1-hydroxy-2-naphthoyl-CoA, 4qij

1,4-Dihydroxy-2-naphthoyl coenzyme A (DHNA-CoA) synthase catalyzes an essential intramolecular Claisen condensation in menaquinone biosynthesis and is an important target for the development of new antibiotics. This enzyme in *Mycobacterium tuberculosis* is cofactor-free and is classified as a type II DHNA-CoA synthase, differing from type I enzymes, which rely on exogenous bicarbonate for catalysis. Its crystal structures in complex with product analogues have been determined at high resolution to reveal ligand-dependent structural changes, which include the ordering of a 27-residue active-site loop (amino acids 107–133) and the reorientation of the carboxy-terminal helix (amino acids 289–301) that forms part of the active site from the opposing subunit across the trimer–trimer interface. These structural changes result in closure of the active site to the bulk solution, which is likely to take place through an induced-fit mechanism, similar to that observed for type I DHNA-CoA synthases. These findings demonstrate that the ligand-dependent conformational changes are a conserved feature of all DHNA-CoA synthases, providing new insights into the catalytic mechanism of this essential tubercular enzyme.

1. Introduction

Tuberculosis causes over one million deaths yearly worldwide and is one of the most fatal infectious diseases (World Health Organization, 2013). The development of new antibacterial drugs against the causal pathogen *Mycobacterium tuberculosis* is urgent because of the limited available drugs and the emergence of multidrug resistance (Dheda *et al.*, 2014). Recently, the biosynthesis of menaquinone, which serves as the essential electron transporter in the respiratory chain of the pathogen, has attracted considerable interest as a drug target. It has been shown that agents that block the biosynthesis of the naphthoquinone vitamin (K_2) are fatal to the tubercular pathogen (Kurosu *et al.*, 2007). More importantly, these menaquinone-blocking antitubercular agents not only effectively eliminate the actively dividing tubercular pathogen but are also able to eradicate the dormant, persistent pathogen in latently infected cells (Dhiman *et al.*, 2009). To date, several essential enzymes of the biosynthetic pathway have been targeted for the development of new drugs (Kurosu *et al.*, 2007; Lu *et al.*, 2008; Fang *et al.*, 2010; Li *et al.*, 2010), including 1,4-dihydroxy-2-naphthoyl-coenzyme A synthase (DHNA-CoA synthase or MenB).

M. tuberculosis MenB (*mt*MenB) is responsible for the conversion of *o*-succinylbenzoyl-CoA (OSB-CoA) to DHNA-CoA (Fig. 1) through a multiple-step intramolecular Claisen condensation reaction. It is a typical crotonase-fold enzyme with a hexameric structure consisting of two eclipsed trimers,

the active site of which is comprised of conserved residues from the N-terminal spiral α/β core domain and the C-terminal helical domain of the opposing subunit across the trimer–trimer interface (Truglio *et al.*, 2003; Johnston *et al.*, 2005). The unique crossing of the C-terminal helical domain over the trimer–trimer interface to form part of the active site of the opposing subunit is found in all structurally characterized MenB orthologues, including those from *Staphylococcus aureus* (Ulaganathan *et al.*, 2007), *Salmonella typhimurium* (PDB entry 3h02; Center for Structural Genomics of Infectious Diseases, unpublished work), *Geobacillus kaustophilus* HTA426 (Kanaujia *et al.*, 2007), *Escherichia coli* (Li *et al.*, 2011; Sun *et al.*, 2012) and *Synechocystis* sp. PCC6803 (Sun *et al.*, 2012). Despite this structural conservation, *mt*MenB is cofactor-free and differs from a large group of MenB orthologues from diverse bacteria, algae and plants, which are dependent on exogenous bicarbonate for catalysis and are classified as type I DHNA-CoA synthases (Jiang *et al.*, 2010; Song & Guo, 2012; Sun *et al.*, 2012). *mt*MenB groups with other orthologues, mainly from actinobacteria and archaea, to form a phylogentically distinctive clade of enzymes that are called type II DHNA-CoA synthases. Interestingly, the exogenous bicarbonate in the type I enzymes occupies an equivalent position to the side-chain carboxylate of a conserved aspartate residue among type II enzymes corresponding to Asp185 of *mt*MenB, which is proposed to serve the role of a general base to initiate the intramolecular Claisen condensation (Jiang *et al.*, 2010; Sun *et al.*, 2012).

The first *mt*MenB crystal structure contained a disordered active-site loop (residues 107–133, called the A-loop), which was thought to become ordered upon substrate binding to seal the active site from the bulk solvent to protect the reaction intermediates (Truglio *et al.*, 2003). Indeed, this active-site loop in the type I MenB from *E. coli* was found to be folded into a β-hairpin in the presence of the substrate analogue *o*-succinylbenzoyl-amino coenzyme A (OSB-NCoA; Li *et al.*, 2011). A similar ordering of the active-site loop was also found in the type I MenB enzymes from *E. coli* and *Synechocystis* sp. PCC6803 when they were bound by the product analogue 1-hydroxy-2-naphthoyl-CoA (HNA-CoA) or salicylyl-CoA (SA-CoA) (Sun *et al.*, 2013). In the product analogue-bound complexes, the C-terminal helix (C-helix) of the enzyme was also found to undergo a significant reorientation to extensively interact with the ordered active-site loop. The altered loop–helix assembly allows additional polar and nonpolar interactions with the coenzyme A moiety of the ligand. These ligand-dependent conformational changes form the basis of a proposed induced-fit catalytic mechanism of intramolecular Claisen condensation (Sun *et al.*, 2013).

However, attempts to observe ordering of the active-site loop have so far failed in type II DHNA-CoA synthases. No conformational changes similar to those observed for the type I DHNA-CoA synthases were found in the *mt*MenB structure determined from crystals soaked with the DHNA-CoA product; no electron density was observed for the aryl part of the product ligand and only its coenzyme A moiety was present in the substrate-binding site (Truglio *et al.*, 2003; Johnston *et al.*, 2005). Another attempt to co-crystallize *mt*MenB with the substrate analogue *o*-succinylbenzoyl-amino coenzyme A (OSB-NCoA) led to a hexameric crystal structure with the two trimers arranged in a staggered rather than the canonical eclipsed configuration, in which the ligand was again invisible and the active-site loop was again disordered (Li *et al.*, 2011).

To further understand the catalytic mechanism of *mt*MenB, this type II enzyme was co-crystallized with the product analogue 1-hydroxy-2-naphthoyl-CoA (HNA-CoA) or salicylyl-CoA (SA-CoA). Interestingly, ligand-dependent conformational changes similar to those observed for the type I enzymes were found in the resulting enzyme complexes, although the aryl moiety of the ligands was only partially visible. This finding shows that the active-site conformational changes are a conserved feature in the catalytic mechanism of all DHNA-CoA synthases and provides a complete active-site structure for the type II *mt*MenB that will facilitate its use as an antitubercular drug target.

2. Materials and methods

2.1. Expression, purification and activity assay of *mt*MenB

The subcloning of the *menB* gene from *M. tuberculosis* into pET-28a has been described previously (Jiang *et al.*, 2010; Chen *et al.*, 2011). *mt*MenB was expressed in *E. coli* BL21 (DE3) as a protein with a hexahistidine tag at the N-terminus with the additional sequence MGSSHHHHHHSSGLVPRGSH at 30°C for 6 h after induction with 200 µ*M* isopropyl β-D-1-thiogalactopyranoside. It was purified to homogeneity by metal-affinity chromatography with a HiTrap Chelating HP column (GE Healthcare) followed by size-exclusion chromatography with a HiPrep 16/60 Sephacryl S-100 column. The concentration of purified protein was measured by the Bradford protein assay using the Coomassie Plus Protein Assay

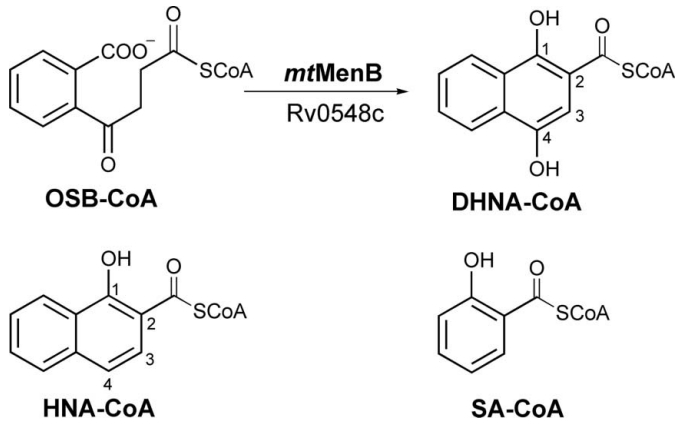

Figure 1
The reaction catalyzed by the DHNA-CoA synthase from the menaquinone-biosynthetic pathway in *M. tuberculosis* (*mt*MenB). 1-Hydroxy-2-naphthoyl-CoA (HNA-CoA) and salicylyl-CoA (SA-CoA) are analogues of the DHNA-CoA product. OSB, *o*-succinyl-1-benzoate; DHNA, 1,4-dihydroxy-2-naphthoate; CoA, coenzyme A.

Table 1
Crystallographic statistics of data collection and refinement.

Values in parentheses are for the highest resolution shell.

	*mt*MenB–SA-CoA	*mt*MenB–HNA-CoA
Data collection		
Space group	$P2_1$	$P2_1$
Unit-cell parameters (Å, °)	a = 91.5, b = 147.7, c = 140.8, α = 90.0, β = 103.5, γ = 90.0	a = 91.5, b = 148.3, c = 141.0, α = 90.0, β = 103.5, γ = 90.0
Total reflections	1712973 (80032)	597288 (52601)
Unique reflections	439236 (21569)	175673 (16438)
Multiplicity	4.0 (3.8)	3.4 (3.2)
Completeness (%)	99.2 (98.6)	94.9 (89.1)
$\langle I/\sigma(I)\rangle$	8.2 (2.2)	11.9 (6.2)
Wilson B factor (Å^2)	16.5	18.0
$R_{\rm merge}$	0.097 (0.70)	0.064 (0.12)
Refinement		
Resolution range (Å)	34.95–1.64 (1.70–1.64)	46.58–2.20 (2.28–2.20)
$R_{\rm work}/R_{\rm free}$	0.15/0.18	0.13/0.18
No. of atoms		
Total	32664	31323
Protein	28083	28080
Ligands	724	732
Water	3856	2511
R.m.s.d., bonds (Å)	0.011	0.008
R.m.s.d., angles (°)	1.08	1.08
Ramachandran plot (%)		
Favoured	98.0	97.4
Allowed	2.0	2.6
Outliers	0	0
Average B factor (Å^2)		
Overall	19.0	20.0
Protein	16.6	18.8
Ligands	33.7	32.4
Solvent	30.5	29.7

Reagent (Pierce). The purified protein was stored in 25 m*M* Tris buffer pH 8.0 containing 10% glycerol at −20°C.

The activity of the recombinant *mt*MenB was assayed as described previously (Jiang *et al.*, 2010; Chen *et al.*, 2011). In the assay, the substrate OSB-CoA was synthesized from (1*R*, 6*R*)-2-succinyl-6-hydroxy-2,4-cyclohexadiene-1-carboxylate (SHCHC) *in situ* with the menaquinone-biosynthetic enzymes MenC and MenE, which were prepared as described previously (Jiang, Cao *et al.*, 2007), before *mt*MenB was added to the reaction mixture to measure the increase in DHNA-CoA absorbance at 392 nm (ε = 4000 M^{-1} cm^{-1}). SHCHC was synthesized chemoenzymatically from chorismic acid with purified EntC (Guo *et al.*, 2008, 2010), MenD (Jiang, Cao *et al.*, 2007) and MenH (Jiang *et al.*, 2008; Jiang *et al.*, 2009; Sun *et al.*, 2014) as described previously (Jiang, Chen *et al.*, 2007). Chorismic acid was prepared using an engineered bacterial strain (Grisostomi *et al.*, 1997).

2.2. Preparation of product analogues and their co-crystallization with *mt*MenB

The product analogues HNA-CoA and SA-CoA were chemically synthesized from coenzyme A and 1-hydroxy-2-naphthoicacid or salicylic acid by a two-step coupling reaction (Guo *et al.*, 2009; Chen *et al.*, 2013). The acids, coenzyme A and the coupling agents *N*-hydroxysuccinimide and *N*,*N*-dicyclohexylcarbodiimide were purchased from Sigma. The CoA thioesters were purified with an Xterra semi-preparative C18 reverse-phase column and a Waters 600E high-performance liquid-chromatography (HPLC) system with a Model 2487 dual-wavelength absorbance detector.

Co-crystallization of *mt*MenB and the product analogue HNA-CoA or SA-CoA was carried out at 294 K using the hanging-drop vapour-diffusion method. The Index HT reagents from Hampton Research were used to screen for crystallization conditions. For co-crystallization with HNA-CoA, *mt*MenB was prepared in solution at 10 mg ml^{-1} and was pre-incubated with 5 m*M* HNA-CoA at 4°C for 1 h before mixing with the Index HT reagents in a 1:1 ratio. Long rod-like crystals appeared in the presence of an Index HT reagent consisting of 0.3 *M* NaCl, 0.1 *M* Tris–HCl pH 8.0, 25% PEG 3350. In a similar co-crystallization, the ligand SA-CoA at a concentration of 2 m*M* was incubated with 10 and 15 mg ml^{-1} protein for 1 h in 20 m*M* Tris–HCl pH 8.0 containing 10% glycerol at 4°C before mixing with the Index HT reagents to screen for crystallization conditions. Using the Index HT reagent 0.2 *M* sodium chloride, 0.1 *M* HEPES pH 8.5, 25% PEG 3350 and an *mt*MenB concentration of 15 mg ml^{-1}, large single crystals with a different shape were found in the co-crystallization with SA-CoA that diffracted to 2.2 Å resolution using a Rigaku R-AXIS IV^{++} diffractometer. These single crystals with high diffraction resolution were flash-cooled in liquid nitrogen with mother liquor supplemented with 20% glycerol as the cryoprotectant for data collection.

2.3. Data collection and structure determination and refinement

All of the X-ray diffraction data from these single crystals were recorded on beamline BL17U of the Shanghai Synchrotron Radiation Facility (SSRF). The images were indexed, integrated and scaled with either *HKL*-2000 (Otwinowski & Minor, 1997) or *iMosflm* (Battye *et al.*, 2011) and *SCALA* (Evans, 2006) in the *CCP*4 suite (Winn *et al.*, 2011). Statistics for the collected data are shown in Table 1.

All of the structures were solved by molecular replacement using *Phaser* (McCoy *et al.*, 2007) with the previously solved *mt*MenB structure (PDB entry 1q51; Truglio *et al.*, 2003) as the initial search model. The obtained models were extended by several rounds of manual fitting with *Coot* (Emsley *et al.*, 2010) and refinement with *PHENIX* (Adams *et al.*, 2010). Non-crystallographic restraints were used at the beginning of the refinement. Translation, libration and screw-rotation displacement (TLS) restraints were used in the final two rounds of refinement (Winn *et al.*, 2001). *eLBOW* (Moriarty *et al.*, 2009) was used to generate and optimize the restraints of the HNA-CoA and SA-CoA ligands for structural fitting and refinement. *MolProbity* (Chen *et al.*, 2010) and *PROCHECK* (Laskowski *et al.*, 1993) were used to assess the overall quality of the refined structures. The *mt*MenB–HNA-CoA and *mt*MenB–SA-CoA structures were refined to high resolutions of 2.2 and 1.64 Å, respectively, with 100% of the amino-acid residues within the allowed region of the Ramanchadran plot and 98% in the preferred region. The refinement statistics are summarized in Table 1. The *Protein Interfaces, Surfaces and*

Assemblies (*PISA*) server (Krissinel & Henrick, 2007) was used to analyze the interactions at protein interfaces and *PyMOL* (DeLano, 2002) was exclusively used to generate the graphical figures. *TopDraw* was used to generate the secondary-structure cartoons (Bond, 2003).

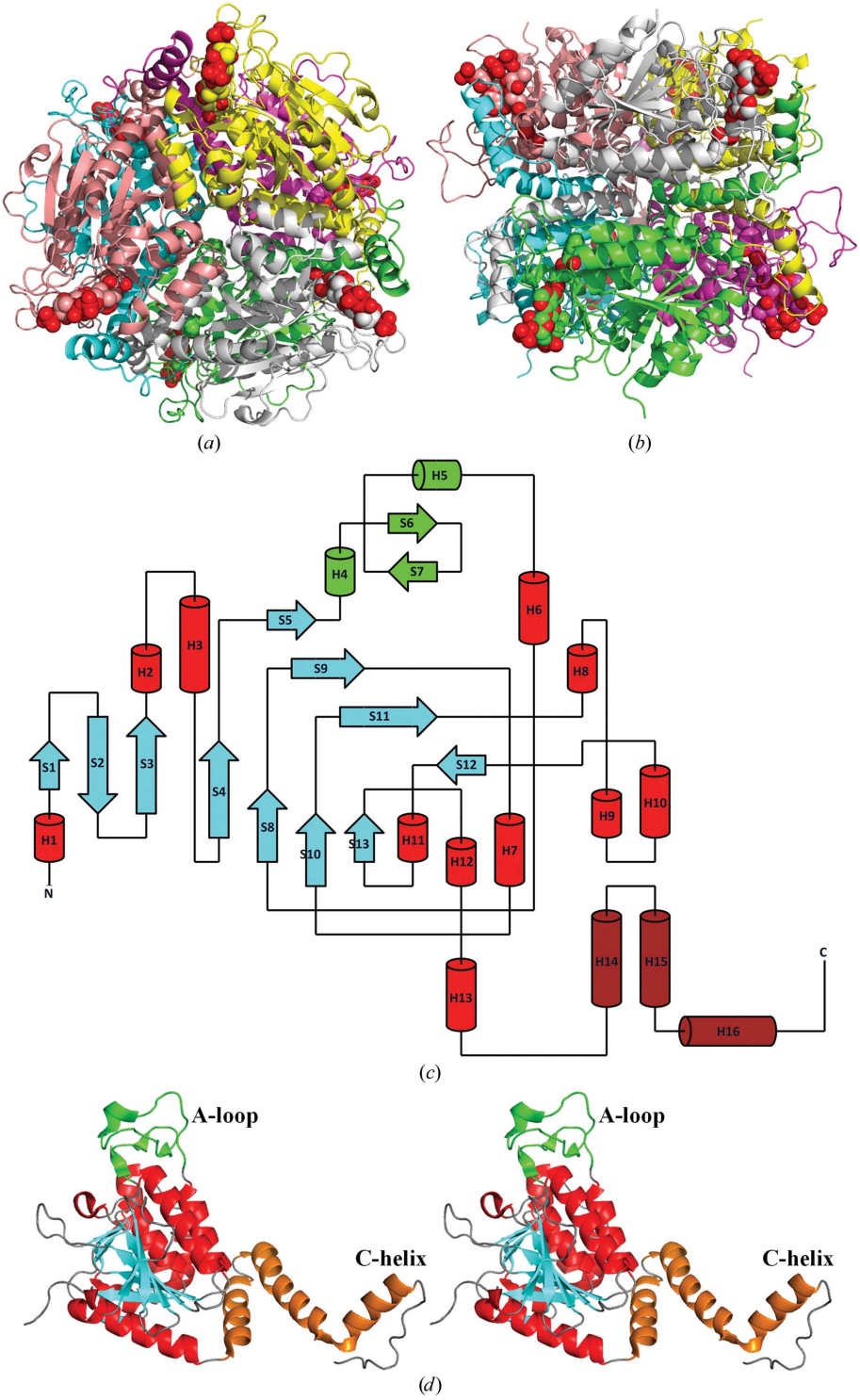

Figure 2
Overall structure of *mt*MenB in complex with a product analogue. (*a*) The hexameric assembly of the *mt*MenB–HNA-CoA complex viewed along the threefold axis of the trimers. The protein is coloured by chain and HNA-CoA is shown as spheres. (*b*) Side view of the hexamer along the trimer–trimer interface. (*c*) Topology diagram of the *mt*MenB subunit. (*d*) Stereo cartoon diagram of the *mt*MenB subunit. In (*c*) and (*d*) the A-loop is coloured green and the C-terminal helical domain is coloured brown. α-Helices and β-pleated sheets in the remaining part of the subunit structure are coloured red and cyan, respectively.

3. Results

3.1. Overall structure

Both the *mt*MenB–HNA-CoA and the *mt*MenB–SA-CoA complex crystal structures belong to space group $P2_1$, with similar unit-cell parameters (Table 1). The structure of *mt*MenB in complex with acetoacetyl-CoA belongs to the same space group with similar but not identical unit-cell parameters (a = 90.4, b = 139.4, c = 142.0 Å; Truglio *et al.*, 2003). There are two hexamers in the asymmetric unit of each structure, which are aligned head-to-tail with their threefold axes tilted at an angle of <5°. These two hexamers present an identical dimer-of-trimers structure in which the trimers are organized in an eclipsed configuration (Figs. 2*a* and 2*b*). The hexamers from the same complex structure or from different complex structures are essentially the same and are superimposable with root-mean-square deviations (r.m.s.d.s) of <0.2 Å over all C^{α} atoms. In addition, all *mt*MenB subunits in the asymmetric units of both complexes are superimposable with each other with an r.m.s.d. of <0.15 Å, demonstrating that the protein molecules are conformationally identical in both complex structures.

Each *mt*MenB subunit is composed of an N-terminal spiral α/β core domain (residues 1–253) and a C-terminal helix domain (residues 254–314), which are characteristic of crotonase-fold enzymes (Engel *et al.*, 1996) and similar to those of the known crystal structures of other MenB orthologues (Figs. 2*c* and 2*d*). The hexahistidine tag and the first 13–17 N-terminal amino-acid residues of each *mt*MenB molecule are disordered. However, all of the remaining residues of each *mt*MenB molecule are well ordered with continuous, well defined electron density for the polypeptide backbone; the electron density for the side chains of most of the amino-acid residues is also very well defined except

for a few surface residues, namely Lys23, Arg26 and Lys95, the terminal atoms beyond the β or γ carbon of which are disordered without electron density. The electron-density OMIT map contoured at 2.0σ is shown in Fig. 3(*a*) for a fragment of the active-site loop (amino acids 107–133) which was disordered in previously determined structures (Truglio *et al.*, 2003; Johnston *et al.*, 2005). Two fragments (Asp121–Asp124 and Asp127–Arg130) in this ordered active-site loop are flexible, with a *B* factor of over 30 Å^2, which is higher than other parts of the polypeptide chain.

3.2. Product-analogue ligands

For each *mt*MenB molecule in the complex structures, a U-shaped CoA thioester ligand is inserted into its active-site crevice with the aryl moiety deeply buried in the enzyme. The adenine dinucleotide phosphate and pantetheinyl moieties of all of the CoA thioester ligands are very well ordered, with clearly discernible electron density. The cysteaminyl part of the small-molecule ligand is less ordered but still recognizable with good electron density, although the terminal S atom and the adjacent methylene group are without electron density in some of the ligands (Fig. 3*a*). However, the aryl moiety of the CoA ligands is poorly defined, with only partial electron density that varies from one ligand to the next. There are always a few discontinuous patches of electron density distributed in the active-site region corresponding to the aryl moiety of the HNA-CoA ligand in the *mt*MenB–HNA-CoA structure. These electron-density patches could not be fitted with water molecules owing to the close distance between them and they always included two density patches within hydrogen-bonding distance of the oxyanion hole or Ser190, where the O atoms of the aryl moiety of the product analogue interact with the corresponding active-site motifs in the type I MenB complex crystal structures. These fragmental electron-density patches became connected in the $2F_o - F_c$ OMIT maps contoured at 1.0σ (Fig. 3*b*) and 0.5σ (Fig. 3*c*) and were thus assigned to the naphthoyl moiety of the ligand. The poor electron density strongly suggests that the aryl moiety is highly flexible with transient interactions with the active-site residues.

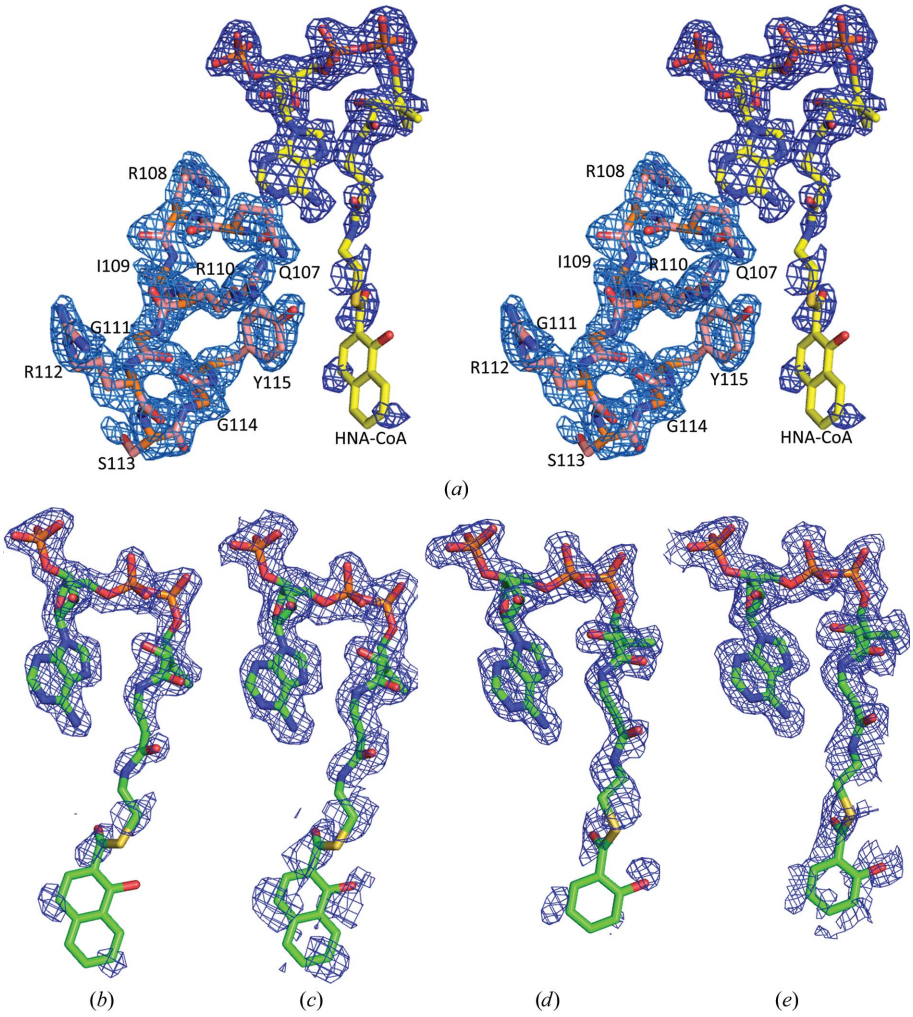

Figure 3
Representative electron-density maps of the crystal structure of *mt*MenB in complex with the product analogues. (*a*) Stereoview of the ($mF_o - DF_c$) OMIT map of DHNA-CoA and part of the A-loop from residues Gln107 to Tyr115 contoured at 2.0σ in chain *A* of the *mt*MenB–HNA-CoA complex. (*b*–*e*) ($2F_o - F_c$) OMIT maps of the small-molecule ligands contoured at 1.0σ (*b*, *d*) and at 0.5σ (*c*, *e*) as a blue mesh in the complex crystal structures. The HNA-CoA ligand in chain *A* of the *mt*MenB–HNA-CoA complex is presented in stick representation in (*b*) and (*c*), while the SA-CoA ligand in chain *F* of the *mt*MenB–SA-CoA complex is presented in stick representation in (*d*) and (*e*).

In the *mt*MenB–SA-CoA structure, with a higher resolution of 1.64 Å, there is essentially no electron density corresponding to the salicylyl moiety in most subunits in the $2F_o - F_c$ OMIT map contoured at 2.0σ. This lack of electron density for the aryl moiety is reminiscent of the absence of electron density for the naphthoyl ring in the structures of *mt*MenB crystals soaked with the DHNA-CoA product (Johnston *et al.*, 2005). Nevertheless, electron density corresponding to the salicylyl moiety of the ligands is found in the $2F_o - F_c$ OMIT maps contoured at 1.0σ and 0.5σ (Figs. 3*d* and 3*e*). On this basis, the SA-CoA thioester ligand was modelled into the *mt*MenB–SA-CoA structure. This model is supported by the fact that the *mt*MenB–SA-CoA structure is essentially the same as the *mt*MenB–HNA-CoA structure in the A-loop ordering and other conformational changes (see below). Compared with HNA-CoA, SA-CoA lacks one aromatic ring that interacts with the hydrophobic patch consisting of three residues (Leu134, Ile13 and Leu137) at the active site and is thus even more flexible, with lower electron density.

3.3. Conformational changes of *mt*MenB after binding the product analogues

One obvious structural change in the *mt*MenB structures in complex with the product analogue is the ordering of the A-loop (residues 107–133) in comparison to the ligand-free *mt*MenB structure or its complexes with acetoacetyl-CoA, DHNA-CoA and OSB-NCoA (Truglio *et al.*, 2003; Johnston *et al.*, 2005; Li *et al.*, 2011). This loop is folded into a β-hairpin that is connected to a 3_{10}-helix on each side through a long random coil (Fig. 3). Superposition of a subunit from the product analogue-bound structures with that of the *mt*MenB–acetoacetyl-CoA complex (PDB entry 1q51; Truglio *et al.*, 2003) reveals another structural change in the former (Fig. 4*a*), which is a significant reorientation of the carboxy-terminal helix, called the C-helix (H16 in Fig. 3). This C-helix reorientation is also obvious when the product analogue-bound structure is compared with *mt*MenB complexes containing other small-molecule ligands. These structural changes are similar to those found for type I MenB orthologues from *E. coli* or *Synechocystis* sp. PCC6803 in complex with an analogue of the substrate or product (Li *et al.*, 2011; Sun *et al.*, 2013). Interestingly, the ordered A-loop of the MenB orthologues of both subtypes contains a similar β-hairpin, which overlap well with each other in a structural superposition (data not shown). This similarity shows that these ligand-dependent conformational changes are an important feature that is conserved among all DHNA-CoA synthases regardless of the different dependence of their catalytic activity on the bicarbonate cofactor.

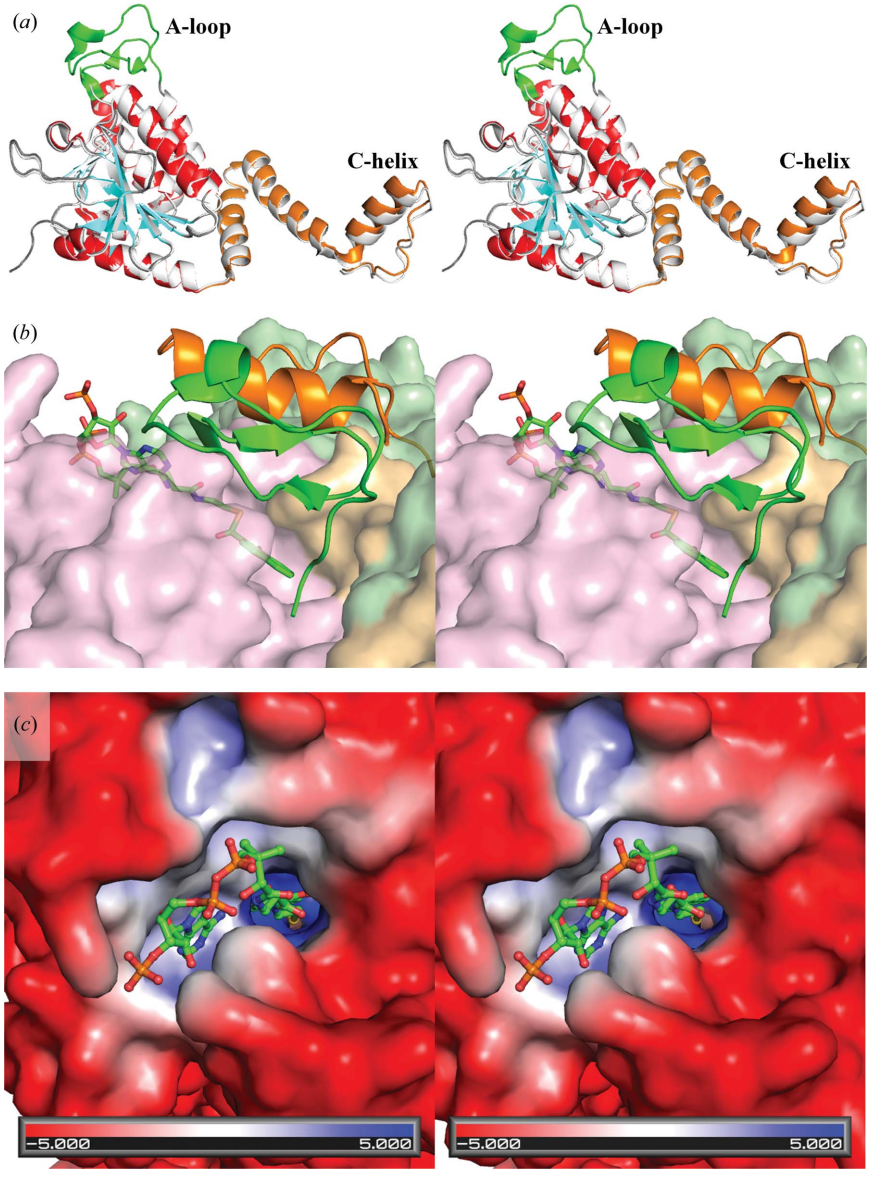

Figure 4
Conformational changes of *mt*MenB in complex with a product analogue. (*a*) Superposition of a typical subunit of *mt*MenB–HNA-CoA and a subunit of *mt*MenB in complex with acetoacetyl-CoA (PDB entry 1q51; grey). The subunit with the ordered A-loop is coloured as in Fig. 3. (*b*) The ordered A-loop and reoriented C-helix block solvent access to the *mt*MenB active site. The *mt*MenB–HNA-CoA hexamer is coloured by chain and shown as a surface representation. (*c*) The narrow ligand-binding channel of *mt*MenB. In (*b*) and (*c*) the HNA-CoA ligand is shown in stick representation, with C, O, N, S and P atoms coloured green, red, blue, yellow and orange, respectively. In (*c*) *mt*MenB is represented as an electrostatic potential surface.

In the three-dimensional hexameric structures of the product analogue-bound *mt*MenB, reorientation of the C-helix moves the helix closer to the active site of the opposing subunit across the trimer–trimer interface, which causes movement of the C^{α} atom of Leu300 by 1.1 and 2.5 Å in comparison to that in ligand-free *mt*MenB and the *mt*MenB–acetoacetyl-CoA complex, respectively. As a result of this reorientation, the C-helix comes into close contact with the newly ordered A-loop and together with the latter seals the active site from the bulk solvent (Fig. 4*b*). These structural changes result in a narrow ligand-binding channel that allows only the cysteaminyl moiety and part of the pantetheionyl moiety to pass through (Fig. 4*c*). The diameter of the narrowest portion of this channel is about 3.9 Å and is significantly smaller than that of the aryl portion of the product analogues or the acyl part of the OSB-CoA substrate, which is then locked in the enzyme active-site cavity after the channel is formed as a result of the conformational changes. The small dimension of the channel strongly suggests that the *mt*MenB–product analogue complexes are formed through an induced-fit mechanism rather than conformational selection.

3.4. Interaction between the A-loop, the C-helix and the ligand

As shown in Fig. 5(*a*), extensive interactions between the ordered A-loop and the C-terminal helical domain in the *mt*MenB–

product analogue complexes are revealed by *PISA* analysis as a result of the ligand-dependent conformational changes. These interactions include a number of hydrogen bonds involving many interfacial amino-acid residues, including the side chains of Arg110, Arg112, Ser113 and Tyr115 and the backbone amides of Arg110 and Gly132 from the ordered A-loop, the side chains of Asp290′ and Arg296′ and the backbone amide of Ala292′ from the C-helix and the side chains of Arg284′ and Tyr287′ and the backbone amide of Met288′ from the penultimate helix (H15 in Fig. 3) in the C-terminal helical domain of the opposing subunit. The total number of these interfacial polar interactions is much higher than that in the corresponding interface in the product-analogue complexes of type I MenB from *E. coli* or *Synechocystis* PCC6803 (Sun *et al.*, 2013), suggesting a stronger interaction between the A-loop and the C-terminal helical domain in type II *mt*MenB structures. The longer A-loop in *mt*MenB compared with type I MenBs is apparently an important factor in this stronger interfacial interaction. Arg110 and Tyr115 are the only conserved nonglycine residues in the long A-loop and their cross-interface hydrogen bonds are also found in type I MenB orthologues in complex with product analogues; most of the other hydrogen-bonding interactions are specific to *mt*MenB and are not found in the type I enzymes. Noticeably, the Arg112 side chain forms a salt bridge with the side chain of Asp260′ located at the end of the C-helix. This ionic interaction, together with the hydrogen-bonding interactions at Ala292′ and Arg296′, provides strong stabilization of the reoriented C-helix.

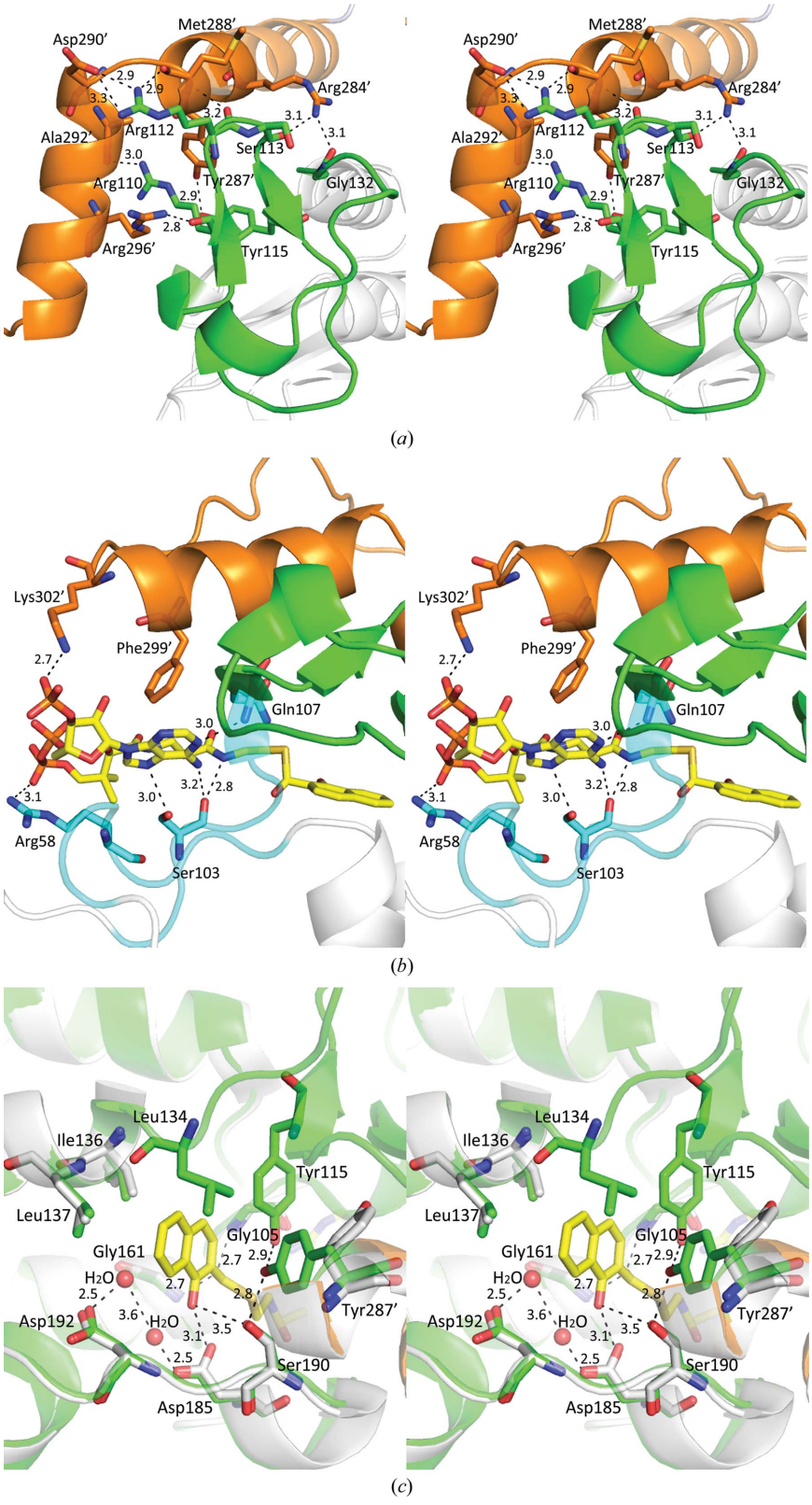

Figure 5
Interactions between the A-loop, the C-terminal helical domain and the product-analogue ligand. (*a*) Stereoview of the interface between the ordered A-loop and the reoriented C-helix in the enzyme–product analogue complexes. (*b*) Stereoview of the new interactions between *mt*MenB and the coenzyme A moiety of the product analogue. Hydrogen bonds between the ligand and Arg58, Ser105 and Gln107 are also present in the *mt*MenB–acetoacetyl-CoA complex. The loop carrying Arg58, Ser105 and Gln107 is coloured cyan. (*c*) Stereoview of the interactions of the active-site residues and the aryl moiety of the HNA-CoA ligand. In (*a*) and (*b*) the A-loop and C-helix are coloured green and orange, respectively, with the interacting amino-acid residues shown in stick representation. In (*b*) and (*c*) the HNA-CoA ligand is shown in stick representation, with C, O, N, S and P atoms coloured yellow, red, blue, salmon and orange, respectively. In (*c*) the *mt*MenB–HNA-CoA structure and the ligand-free *mt*MenB (PDB entry 1q52) are shown in green and grey, respectively, with the active-site residues shown in stick representation. Residues labelled with a prime are from a different subunit, which crosses the trimer–trimer interface to form part of the active site of the opposing subunit. Dashed lines denote hydrogen bonds with distances in Å.

The ligand-dependent conformational changes bring about a couple of additional stabilizing interactions with the coenzyme A moiety of the ligands (Fig. 5*b*). The first is a salt bridge formed between the side chain of Lys302′ from the reoriented C-helix and the adenylate 3′-phosphate of the ligand, and the other is a hydrophobic contact between the aromatic benzene ring of Phe299′ from the reoriented C-helix and the aromatic adenine ring of the ligand at an almost perpendicular angle. This hydrophobic contact is ∼2.6 Å in the product analogue-bound *mt*MenB and is ∼4.0 Å in *mt*MenB complexed with acetoacetyl-CoA. Both additional interactions with the coenzyme A moiety are also observed for the type I MenB orthologues in complex with product analogues (Sun *et al.*, 2013). However, the assembly of the ordered A-loop and the reoriented C-helix forms one additional hydrogen bond to the coenzyme A moiety of the ligand in *E. coli* MenB, suggesting stronger binding for the ligands in the type I enzyme. This difference may underline the fact that the HNA-CoA ligand is firmly bound with well defined electron density in *E. coli* MenB (Sun *et al.*, 2013) but is highly flexible in *mt*MenB.

3.5. Active site

As described previously, the most significant change to the enzyme active site is its closure to the bulk solution as a result of the A-loop ordering and C-helix reorientation. The ordering of the A-loop allows the Tyr115 side chain to form a hydrogen bond to the side-chain phenolic hydroxyl group of another active-site residue Tyr287′ from the opposing subunit across the trimer–trimer interface, which leads to significant reorientation of the Tyr287′ side chain in comparison to the ligand-free *mt*MenB or its complex with acetoacetyl-CoA or DHNA-NCoA (Fig. 5*c*). As a result, a new hydrogen-bonding network is formed involving these two tyrosine residues as well as Asp185 and Ser190. The positions and orientations of the other active-site residues, however, are not significantly changed. These unchanged residues include Gly105 and Gly161, the backbone amides of which form an oxyanion hole and interact with the product analogues at the O atom of the carboxyl group at the C2 position, Leu134, Ile136 and Leu137, the side chains of which form hydrophobic interactions with the product analogue ligands, Ser190, the side-chain hydroxyl group of which interacts with the C1–OH of the ligands and forms part of the hydrogen-bonding network involving Tyr115 and Tyr287′, and the two acidic residues Asp185 and Asp192.

3.6. Binding affinity of *mt*MenB for HNA-CoA

The binding of the DHNA-CoA product by MenB orthologues from various bacterial species has been shown to cause drastic changes in the electronic absorption spectrum of the small-molecule ligand (Chen *et al.*, 2011). *E. coli* MenB has also been shown to bind HNA-CoA tightly with a dissociation constant of 0.11 μ*M* and to cause similar spectral changes in its UV–Vis spectrum (Chen *et al.*, 2011). The spectral changes mainly result from the ionizing hydrogen-bonding interaction occurring at the C1–OH of the ligand, which is strong when the ligand is bound to the type I MenB orthologues from *E. coli* or *Synechocystis* sp. PCC6803 (Sun *et al.*, 2013). Based on these observations, the electronic spectrum of HNA-CoA was also found to change from a single peak at 372 nm in its free state to a double peak at 400 and 418 nm when it was bound by *mt*MenB (Fig. 6*a*).

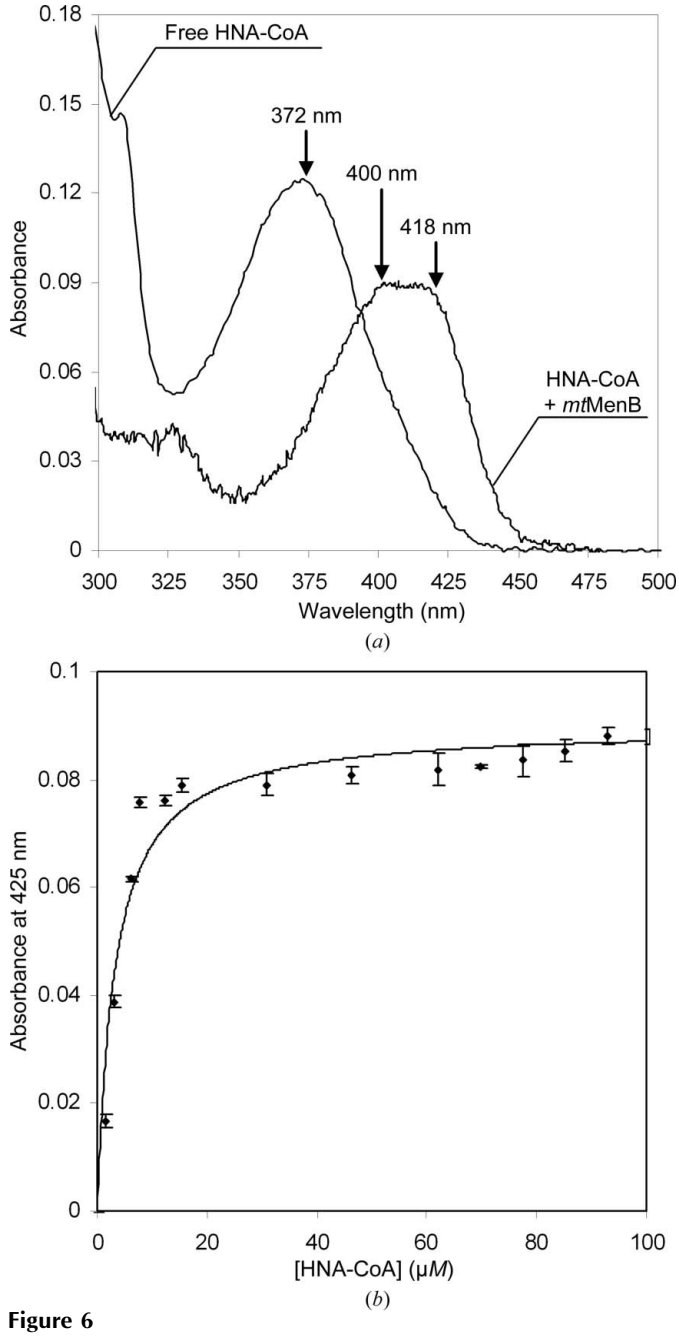

Figure 6
Determination of the binding affinity of *mt*MenB for HNA-CoA. (*a*) UV–Vis spectra of HNA-CoA before and after binding to *mt*MenB. The concentration of HNA-CoA was 40 μ*M* in its free form and 7.8 μ*M* in the presence of 10 μ*M* *mt*MenB. The spectrum of free HNA-CoA is the same as that shown in a previous study (Chen *et al.*, 2011). (*b*) Titration of *mt*MenB with HNA-CoA. In the titration, *mt*MenB was fixed at 10 μ*M* while HNA-CoA was varied from 0 to 100 μ*M*. The protein absorbance has been subtracted in the presented results. All of the spectral measurements were carried out in 50 m*M* potassium phosphate pH 8.0. The solid line in (*b*) is the curve-fitting result using a saturation growth model.

Spectroscopic titration of *mt*MenB with HNA-CoA was used to determine the strength of their binding interaction, using the characteristic absorption at 425 nm to indicate formation of the enzyme–ligand complex. As shown in Fig. 6(*b*), curve-fitting of the titration curve gives a dissociation constant (K_d) of 2.9 $\pm$ 0.3 μM, which is 25-fold higher than that of the *E. coli* MenB complex with HNA-CoA (Chen *et al.*, 2011). This affinity difference is fully consistent with the fact that HNA-CoA is highly flexible with partial electron density for its aryl moiety in complex with *mt*MenB (Figs. 2*c* and 2*d*) but is rigid with well defined electron density in complex with *E. coli* MenB (Sun *et al.*, 2013).

4. Discussion

On co-crystallization with the product analogue HNA-CoA or SA-CoA, *mt*MenB is shown to undergo ligand-dependent conformational changes that include ordering of the A-loop and reorientation of the C-helix. These conformational changes significantly alter the active site by sealing it from the bulk solution and allow more stabilizing interactions with the small-molecule ligands. When the structurally similar OSB-CoA substrate is bound to the active site, the enzyme is expected to undergo the same conformational changes to protect the reactive reaction intermediates from the bulk solution by causing a similar closure of the active site. As such, these ligand-dependent conformational changes are an integral part of the enzyme catalytic mechanism. Similar structural changes are found for the type I MenB orthologues in complex with an analogue of either the OSB-CoA substrate or the DHNA-CoA product (Li *et al.*, 2011; Sun *et al.*, 2013), demonstrating that these conformational changes are conserved among all DHNA-CoA synthases regardless of their phylogenetically divergent dependence on the bicarbonate cofactor.

The electron density for the aryl moiety of the product-analogue ligands is poor in the *mt*MenB complex crystal structures compared with the same ligands in type I MenB orthologues (Sun *et al.*, 2013). This is consistent with the weaker affinity of *mt*MenB for the product analogue HNA-CoA, with a 25-fold higher K_d compared with the type I *E. coli* MenB (Fig. 6). The presence of the ligand in the active site and the associated structural changes in *mt*MenB clearly differs from their absence in *mt*MenB single crystals soaked with the DHNA-CoA product (Johnston *et al.*, 2005). One possible explanation for this difference is that the DHNA-CoA product might have been hydrolyzed or damaged during the soaking process or data collection owing to the chemical instability of DHNA-CoA, which has been shown to be easily oxidized by air in neutral buffer solution (Chen *et al.*, 2011). Alternatively, the ligand-dependent conformational changes might have been prohibited by the crystal-packing interactions or by steric hindrance associated with the structural changes even if DHNA-CoA were successfully soaked intact into the enzyme active site. As a result, the aryl moiety of the product ligand was too flexible to be visible owing to the lack of stabilizing interactions associated with the structural changes. In the consideration of these possibilities, co-crystallization may be the key to the successful observation of the ligand-dependent structural changes in the product analogue-bound *mt*MenB structures. The DHNA-CoA product is not suitable for co-crystallization because of its chemical instability.

In comparison to the absence of A-loop ordering or C-helix reorientation in the *mt*MenB–acetoacetyl-CoA complex (Truglio *et al.*, 2003), these structural changes observed in the product analogue-bound *mt*MenB structures are clearly caused by the aryl moiety of the small-molecule ligands. The causal interaction is most likely to be the hydrophobic interaction of the aryl group with the active-site hydrophobic patch consisting of Leu134, Ile136 and Leu137 (Fig. 5*c*) that are directly connected to the A-loop. This hydrophobic interaction may trigger ordering of the A-loop, which is subsequently stabilized by extensive interaction with the C-helix, resulting in significant reorientation of the latter. This mechanism of ligand-dependent conformational changes is similar to the sequential induced-fit mechanism proposed for the type I MenB orthologues (Sun *et al.*, 2013). As mentioned previously, the ligand-dependent conformational changes have to undergo an induced-fit mechanism because the ligand-binding conformation does not allow the aryl moiety of the ligand to enter or exit the active site once it has formed (Fig. 4*c*).

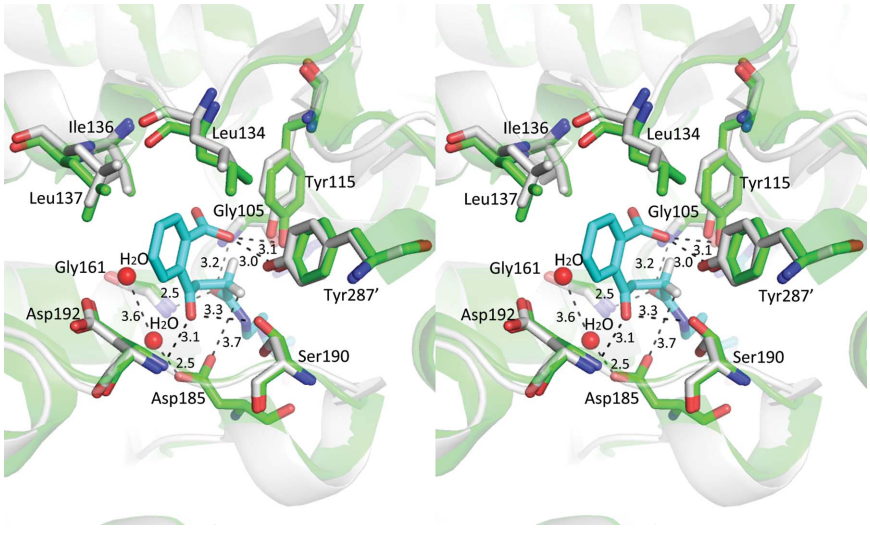

Figure 7
Stereoview of the substrate analogue OSB-NCoA modelled into the active site of the *mt*MenB–HNA-CoA complex. The substrate analogue is from *E. coli* MenB in complex with OSB-NCoA (PDB entry 3t88) and is shown in stick representation, with H, C, N, P and O atoms shown in white, cyan, blue, brown and red, respectively. *mt*MenB and *E. coli* MenB are superimposed and are coloured green and grey, respectively. All of the active-site residues are from *mt*MenB and are shown in stick representation. Dashed lines denote hydrogen bonds with distances in Å.

Compared with the open active site in ligand-free *mt*MenB or its complex with acetoacetyl-CoA (Truglio *et al.*, 2003), the closed active site in the product analogue-bound *mt*MenB structures is more relevant to enzyme catalysis because the closed cavity protects the reactive intermediate from the environmental reactants and allows the multi-step intramolecular Claisen condensation to take place without interference from solvent molecules. To understand how this new active site interacts with the substrate, the OSB-NCoA substrate analogue was manually docked into the closed *mt*MenB active site by overlapping the *mt*MenB–HNA-CoA complex structure with the OSB-NCoA complex of the MenB orthologue from *E. coli* (PDB entry 3t88; Li *et al.*, 2011). The *E. coli* MenB polypeptide and HNA-CoA were then deleted to place the substrate analogue OSB-NCoA in the closed *mt*MenB active site. As shown in Fig. 7, the modelled active site is similar to that of the type I *E. coli* MenB in complex with OSB-NCoA.

In the modelled structure, the hydrophobic patch consisting of Leu134, Ile136 and Leu137 still interacts with the hydrophobic part of the benzoyl ring of the substrate analogue, similar to the hydrophobic interaction with the product analogues (Fig. 5*c*). In addition, the side-chain carboxylate of Asp185 is 3.7 Å away from the *pro*-R α-proton of the succinyl amide moiety of the ligand and is therefore suitable for α-proton abstraction from OSB-CoA to generate an enolate for nucleophilic addition to the C1 carboxyl group of the benzoyl ring in enzyme catalysis. This proposed role for Asp185 is consistent with previous mutational results that showed that this residue is essential to the enzymatic catalysis (Truglio *et al.*, 2003). Moreover, the phenolic hydroxyl groups of both Tyr115 and Tyr287′, the former of which is from the ordered A-loop and the latter of which is significantly reoriented in the product analogue-bound *mt*MenB structures (Fig. 5*c*), are within hydrogen-bonding distances of the C1 carboxylate on the aromatic moiety of the substrate analogue. These two tyrosine residues are thus believed to form the oxyanion hole responsible for stabilization of the tetrahedral oxyanion intermediate formed after nucleophilic attack of the enolate on the C1 carboxyl group in the Claisen condensation reaction, similar to the proposed role for the corresponding tyrosine residues in the type I *E. coli* MenB (Li *et al.*, 2011). Based on these analyses, a catalytic mechanism is proposed for *mt*MenB as shown in Fig. 8.

This proposed *mt*MenB catalytic mechanism is consistent with that proposed for catalysis by type I MenB orthologues, in which a bicarbonate plays the same role as a catalytic base as the side chain of Asp185 in *mt*MenB (Jiang *et al.*, 2010; Sun *et al.*, 2012, 2013; Song & Guo, 2012), leading to a unified catalytic mechanism for both type I and type II DHNA-CoA synthases. Indeed, the Asp185 side-chain carboxylate occupies a position equivalent to the bound bicarbonate in the type I MenB orthologues from either *E. coli* or *Synechocystis* sp. PCC6803 in a structural superposition (data not shown). Thus far, the unified catalytic mechanism is consistent with all of the experimental facts collected for all DHNA-CoA synthases, including the bicarbonate dependence of the type I MenB orthologues and the preferential abstraction of the *pro*-R α-proton from the OSB-CoA substrate (Igbavboa & Leistner, 1990). It differs from an alternative catalytic mechanism in which the C1 carboxylate of OSB-CoA was proposed to serve as the catalytic base for α-proton abstraction (Truglio *et al.*, 2003; Li *et al.*, 2011). In this alternative mechanism, the *pro*-S rather than the *pro*-R α-proton has to be abstracted from the substrate, contrary to experimental observations (Igbavboa & Leistner, 1990). In addition, this alternative mechanism is unable to explain the dependence of the type I DHNA-CoA synthases on exogenous bicarbonate.

In summary, high-resolution structures of *M. tuberculosis* MenB have been successfully determined in complex with the product analogue HNA-CoA or SA-CoA. For the first time, this type II MenB orthologue is shown to undergo ligand-dependent conformational changes similar to those found for the type I MenB orthologues. This finding supports the notion that the ligand-dependent conformational changes, which form the basis of an induced-fit catalytic mechanism, are conserved, allowing a unified catalytic mechanism to be proposed for all DHNA-CoA synthases. More importantly, the mechanistic insights gained in this study and the details of

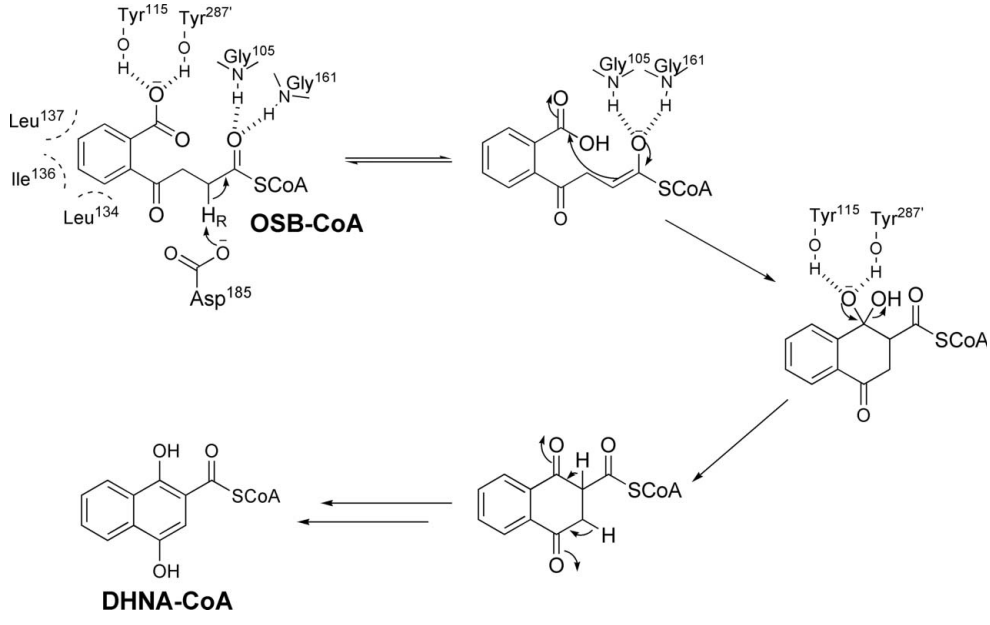

Figure 8
Proposed catalytic mechanism of the intramolecular Claisen condensation catalyzed by *mt*MenB.

the product analogue-bound crystal structures may guide the design of new antitubercular inhibitors against this essential mycobacterial enzyme.

We are grateful for access to beamline BL17U1 at SSRF, Shanghai, People's Republic of China and thank the beamline staff for technical support. This work was supported by GRF601413, GRF601203 and FSGRF13SC01 from the Research Grants Council of the HKSAR government.

References

Adams, P. D. *et al.* (2010). *Acta Cryst.* D**66**, 213–221.
Battye, T. G. G., Kontogiannis, L., Johnson, O., Powell, H. R. & Leslie, A. G. W. (2011). *Acta Cryst.* D**67**, 271–281.
Bond, C. S. (2003). *Bioinformatics*, **19**, 311–312.
Chen, V. B., Arendall, W. B., Headd, J. J., Keedy, D. A., Immormino, R. M., Kapral, G. J., Murray, L. W., Richardson, J. S. & Richardson, D. C. (2010). *Acta Cryst.* D**66**, 12–21.
Chen, M., Jiang, M., Sun, Y., Guo, Z.-F. & Guo, Z. (2011). *Biochemistry*, **50**, 5893–5904.
Chen, M., Ma, X., Chen, X., Jiang, M., Song, H. & Guo, Z. (2013). *J. Bacteriol.* **195**, 2768–2775.
DeLano, W. L. (2002). *PyMOL*. http://www.pymol.org.
Dheda, K., Gumbo, T., Gandhi, N. R., Murray, M., Theron, G., Udwadia, Z., Migliori, G. B. & Warren, R. (2014). *Lancet Respir. Med.* **2**, 321–338.
Dhiman, R. K., Mahapatra, S., Slayden, R. A., Boyne, M. E., Lenaerts, A., Hinshaw, J. C., Angala, S. K., Chatterjee, D., Biswas, K., Narayanasamy, P., Kurosu, M. & Crick, D. C. (2009). *Mol. Microbiol.* **72**, 85–97.
Emsley, P., Lohkamp, B., Scott, W. G. & Cowtan, K. (2010). *Acta Cryst.* D**66**, 486–501.
Engel, C. K., Mathieu, M., Zeelen, J. P., Hiltunen, J. K. & Wierenga, R. K. (1996). *EMBO J.* **19**, 5135–5145.
Evans, P. (2006). *Acta Cryst.* D**62**, 72–82.
Fang, M., Toogood, R. D., Macova, A., Ho, K., Franzblau, S. G., McNeil, M. R., Sanders, D. A. R. & Palmer, D. R. (2010). *Biochemistry*, **49**, 2672–2679.
Grisostomi, C., Kast, P., Pulido, R., Huynh, J. & Hilvert, D. (1997). *Bioorg. Chem.* **25**, 297–305.
Guo, Z.-F., Jiang, M., Zheng, S. & Guo, Z. (2008). *Org. Lett.* **10**, 649–652.
Guo, Z.-F., Jiang, M., Zheng, S. & Guo, Z. (2010). *Bioorg. Med. Chem. Lett.* **20**, 3855–3858.
Guo, Z.-F., Sun, Y., Zheng, S. & Guo, Z. (2009). *Biochemistry*, **48**, 1712–1722.
Igbavboa, U. & Leistner, E. (1990). *Eur. J. Biochem.* **192**, 441–449.
Jiang, M., Cao, Y., Guo, Z.-F., Chen, M., Chen, X. & Guo, Z. (2007). *Biochemistry*, **46**, 10979–10989.
Jiang, M., Chen, M., Cao, Y., Yang, Y., Sze, K. H. & Guo, Z. (2007). *Org. Lett.* **9**, 4765–4767.
Jiang, M., Chen, X., Guo, Z.-F., Cao, Y., Chen, M. & Guo, Z. (2008). *Biochemistry*, **47**, 3426–3434.
Jiang, M., Chen, M., Guo, Z.-F. & Guo, Z. (2010). *J. Biol. Chem.* **285**, 30159–30169.
Jiang, M., Chen, X., Wu, X.-H., Chen, M., Wu, Y.-D. & Guo, Z. (2009). *Biochemistry*, **48**, 6921–6931.
Johnston, J. M., Arcus, V. L. & Baker, E. N. (2005). *Acta Cryst.* D**61**, 1199–1206.
Kanaujia, S. P., Ranjani, C. V., Jeyakanthan, J., Baba, S., Kuroishi, C., Ebihara, A., Shinkai, A., Kuramitsu, S., Shiro, Y., Sekar, K. & Yokoyama, S. (2007). *Acta Cryst.* F**63**, 103–105.
Krissinel, E. & Henrick, K. (2007). *J. Mol. Biol.* **372**, 774–797.
Kurosu, M., Narayanasamy, P., Biswas, K., Dhiman, R. & Crick, D. C. (2007). *J. Med. Chem.* **50**, 3973–3975.
Laskowski, R. A., MacArthur, M. W., Moss, D. S. & Thornton, J. M. (1993). *J. Appl. Cryst.* **26**, 283–291.
Li, H.-J., Li, X., Liu, N., Zhang, H., Truglio, J. J., Mishra, S., Kisker, C., Garcia-Diaz, M. & Tonge, P. J. (2011). *Biochemistry*, **50**, 9532–9544.
Li, X., Liu, N., Zhang, H., Knudson, S. E., Slayden, R. A. & Tonge, P. J. (2010). *Bioorg. Med. Chem. Lett.* **20**, 6306–6309.
Lu, X., Zhang, H., Tonge, P. J. & Tan, D. S. (2008). *Bioorg. Med. Chem. Lett.* **18**, 5963–5966.
McCoy, A. J., Grosse-Kunstleve, R. W., Adams, P. D., Winn, M. D., Storoni, L. C. & Read, R. J. (2007). *J. Appl. Cryst.* **40**, 658–674.
Moriarty, N. W., Grosse-Kunstleve, R. W. & Adams, P. D. (2009). *Acta Cryst.* D**65**, 1074–1080.
Otwinowski, Z. & Minor, W. (1997). *Methods Enzymol.* **276**, 307–326.
Song, H. & Guo, Z. (2012). *Sci. China Chem.* **55**, 98–105.
Sun, Y., Song, H., Li, J., Jiang, M., Li, Y., Zhou, J. & Guo, Z. (2012). *Biochemistry*, **51**, 4580–4589.
Sun, Y., Song, H., Li, J., Li, Y., Jiang, M., Zhou, J. & Guo, Z. (2013). *PLoS One*, **8**, e63095.
Sun, Y., Yin, S., Feng, Y., Li, J., Zhou, J., Liu, C., Zhu, G. & Guo, Z. (2014). *J. Biol. Chem.* **289**, 15867–15879.
Truglio, J. J., Theis, K., Feng, Y., Gajda, R., Machutta, C., Tonge, P. J. & Kisker, C. (2003). *J. Biol. Chem.* **278**, 42352–42360.
Ulaganathan, V., Agacan, M. F., Buetow, L., Tulloch, L. B. & Hunter, W. N. (2007). *Acta Cryst.* F**63**, 908–913.
Winn, M. D. *et al.* (2011). *Acta Cryst.* D**67**, 235–242.
Winn, M. D., Isupov, M. N. & Murshudov, G. N. (2001). *Acta Cryst.* D**57**, 122–133.
World Health Organization (2013). *Global Tuberculosis Report 2013.* Geneva: World Health Organization. http://www.who.int/tb/publications/global_report/en/.